Visualization and comparison of DEM-derived parameters. Application to volcanic areas

Massimiliano Favalli[1] and Alessandro Fornaciai[1,2]

[1] Istituto Nazionale di Geofisica e Vulcanologia, via della Faggiola 32, 56126 Pisa, Italy

[2] Dipartimento di Fisica e Astronomia, Alma Mater Studiorum - Università di Bologna, Viale Carlo Berti Pichat 8, 40127 Bologna, Italy

Abstract

Digital Elevation Models (DEMs) are fruitfully used in volcanology as the topographic base for mapping and quantifying volcanic landforms. The increasing availability of free topographic data on the web, decreasing production costs for high-accuracy data and advances in computer technology, has triggered rapid growth of the number of DEM users in the volcanological community. DEMs are often visualized only as hill-shaded maps, and while this is among the major advantages in using them, the possibility of deriving a very large number of parameters from a single grid of elevation data makes DEMs a powerful tool for morphometric analysis. However, many of these parameters have almost the same informative content, and before starting to elaborate topographic data it is recommended to know *a-priori* what parameters best visualize the investigated landform, and therefore what is necessary and what is redundant. In this work, we review a number of analytical procedures used to parameterize and represent DEMs. A LIDAR-derived DEM matrix acquired over the Valle del Bove valley, on Mt. Etna, is used as test-case elevation data for deriving the parameters. We first review well known parameters such as hill-shading, slope and aspect, curvature, and roughness, before extending the review to some less common parameters such as Sky View Factor (*SVF*), openness, and Red Relief Image Maps (RRIM). For each parameter a description is given emphasizing how it can be used for identifying and delimiting specific volcanic elements. The analyzed surface parameters are then cross-

compared in order to infer which of them is most uncorrelated, and the results are represented in the form of a correlation matrix. Finally, the reviewed DEM-derived parameters and the correlation matrix are used for analyzing the volcanic landforms of two case studies: Michoacán-Guanajuato volcanic field and a phonolitic lava flow at the Island of Tenerife.

Keywords. Digital elevation model, surface parameters, correlation matrix, volcanic field, lava flow

1. Introduction

Geomorphometry is crucial for understanding the relationship between the present shape of landforms and their morphogenetic processes. Over the last decade, digital elevation models (DEMs) have been used increasingly for morphometric analysis in volcanology, thanks to the advancements in remote-sensing and photogrammetry methods for generating DEM as well as to the increasing availability of web-shared DEMs.

Airborne and terrestrial laser scanning and ranging technologies are largely used to provide topographic data with high resolution (e.g. Favalli et al., 2009; Tarolli, 2014). DEMs with high accuracy can also be produced from images taken with a consumer-grade camera by using open-source or low-cost software implementing structure from motion (SfM) methods (e.g. Favalli et al., 2012; Westoby et al., 2012; James and Robson, 2012; Kolzenburg et al., 2016).

Several high-resolution topographic datasets are freely available as well as appropriate tools for processing such huge volumes of data (e.g. http://www.opentopography.org). There are also many DEMs with countrywide coverage: for example the National Elevation Dataset for US (http://seamless.usgs.gov), TINITALY for Italy (Tarquini et al., 2012) and a 10-m resolution DEM for Japan (http://fgd.gsi.go.jp/view). With (almost) global coverage, the 90-m Shuttle Radar Topography Mission DEM (SRTM; http://www2.jpl.nasa.gov/srtm) and the 30-m Advanced

Spaceborne Thermal Emission and Reflection Radiometer (ASTER) Global DEM (GDEM; http://www.gdem.aster.ersdac.or.jp) are freely downloadable.

A common, general workflow for land surface DEM-based morphometric analysis requires an initial detailed identification and delineation of surface-specific elements, i.e. pits, peaks, ridge lines, course lines and breaks lines. This is often done through human-made analysis from one or more DEM-derived surface parameters. Olaya (2009) defined surface parameters as measures that can be derived directly from a DEM without further knowledge of the area represented. Common surface parameters are for example DEM-derived slope, aspect and curvature which are generally represented as maps.

The high detail and spatial extension of the data supplied by the new technologies demand an effort in suitably visualizing this wealth of data. Finding proper techniques to adequately parameterize DEMs and represent maps is required for effective land-surface quantitative analysis and, currently, it is pursued through multidisciplinary approaches (e.g. Buckley et al., 2004; Chiba et al., 2008; Kennelly, 2008; Mitasova et al., 2012).

In this work, we review a number of analytical procedures used to parameterize and represent DEMs. For each described parameter, we emphasize which are the specific elements of land surface that are better highlighted. We first introduce some well-known parameters, such as hill-shaded maps, slope and aspect maps, curvature maps, roughness maps, and then we extend the review to some less common parameters such as Sky View Factor (*SVF*) maps, openness maps, Red Relief Image Maps (RRIM). As a test case, we use a 1200×1200 m LiDAR-derived DEM matrix acquired over the Valle del Bove valley, on Mt. Etna, during the June 2007 airborne survey with spatial resolution of 1 m (for details see Favalli et al., 2009). The location and an aerial photo of the test area is shown in Fig. 1a, b and c. The test area is characterized by the presence of two main volcanic landforms: i) a well-preserved, relatively smooth, scoria cone; and ii) lava channels variously superimposed.

Parameters are derived directly from the DEM without additional inputs using a C++ code developed *ad-hoc* that generates all maps in one shot, without assistance. The code and batch file

are not designed to be fast for real time elaboration, but to run in background. Since many of the surface parameters reviewed here have the same informative content even if in a slightly different form, it is relevant to evaluate whether or not two maps contain redundant information, before starting time-consuming computer routines. For this reason, the here reviewed surface parameters are cross-compared in order to infer which of them are most uncorrelated. The results are represented as a correlation matrix that can be used for discarding redundant maps. Finally, the highly uncorrelated parameters are used for carrying out a morphometric analysis and test a semi-automatic classification of specific features in two volcanic areas with different and heterogeneous topography: i) a portion of ASTER DEM acquired over the Michoacán -Guanajuato volcanic field; and ii) a portion of 10-m resolution DEM of a phonolitic lava flow on Tenerife Island produced by GRAFCAN (2009).

2. Grid to grayscale image conversion and image enhancement

DEMs and derivative maps are generally in a grid format with values represented by single or double precision numbers. To be displayed, grids must be converted into simple gray-scale or color-map images (8-bit images) in order to associate proper shades of colors to grid data values.

The first way to represent a grid is simply to convert it into a grayscale image where the gray tones correspond to grid values. This can be done using a linear map function, which converts the minimum-maximum (min-max) range values of the grid into the 0–255 standard range of a normal 8-bit grayscale image. However, this will have a very low visual impact if the grid values are not "almost uniformly" distributed in the range (min, max) as can be seen in Fig. 1d.

An image can be visually enhanced by stretching its histogram using various techniques. An image histogram is a graphical representation of the number of pixels in an image as a function of their intensity. The greater the histogram stretch, the greater the contrast of the image. Although histogram stretching may produce unrealistic effects, they turn out to be useful for scientific purposes since false-color images are often able to better highlight specific features. However,

histogram stretching can also produce undesirable effects (i.e. visible image gradient) when applied to 8-bit or lower color images. For this reason, it is recommended to apply the histogram stretching on the single or double precision numeric values of the original grid and afterwards convert it into an image.

Area equalization is another commonly used technique for image enhancement in which each intensity class is represented by the same number of pixels (that is by the same area). This produces a histogram which is as flat as possible (Fig. 1e). As a consequence, each gray-scale tone is "almost" equally represented and the resulting images appear well contrasted (Fig. 1e). However the gray tone range is no longer directly proportional to the range of values of the original input data. This raises problems when attaching quantity values to the legend of the output image map.

On the contrary, by cutting-off the histogram at upper and lower threshold values, the overall histogram shape and a direct proportionality between grayscale tones and original data values can be maintained (Fig. 1f). Upper and lower cut-offs can be either external meaningful values or calculated from the statistical distribution of the values in the original grid. For example, clipping the grid values between μ - 2.5σ and μ + 2.5σ (where μ is the average pixel value and σ is the standard deviation) usually provide well-contrasted images (e.g. Fig. 1f). However different areas have different statistics and therefore the maps of different regions derived using the 2.5σ stretching have different legends and are not directly comparable. On the contrary, the same histogram cut-offs produce comparable maps though the resulting image contrast and map readability might not be optimal.

Broadly speaking, a definitive optimal way to convert grids into gray-scale images cannot be recommended. Based on our experience, linearly stretching grid values to the 0–255 grayscale values provides unusable maps in many cases, because of the low contrast in the resulting image. Area equalization works in many occasions but sometimes produces maps that appear too saturated. The 2.5σ clipping gives acceptable results in most cases and often provides better results than the equal area equalization. These grayscale images can be considered as a first mandatory step to produce building blocks for more elaborated colored maps. Indeed, they can be composed as a

simple HSV (Hue–Saturation–Value) image in order to create a great variety of maps. In the following, all the maps, other than hillshaded and aspect maps, will be represented with 2.5σ clipping, which in our opinion gives the best visual enhancement in general, while keeping the shape of histogram.

3. DEM-derived surface parameters

3.1. DEM and derivatives

In simple terms, a land surface can be described as $z=f(x,y)$, which means that elevation z depends solely on planar coordinates x and y (Cayley, 1859). In computer science, land surfaces are commonly presented as Digital Elevation Models (DEMs), a gridded set of points in Cartesian space attributed with elevation values that describe the Earth's ground surface (Wilson, 2012). This means that heights are available at each point in the area of interest (Hengl and Evans, 2009) with the exclusion of no data cells.

To derive some basic DEM parameters such as hill-shade, slope and aspect, the derivatives of the DEM in each point must be calculated. Since the DEM is a discrete square mesh, DEM gradients can be calculated by applying some filter masks to the DEM matrix. The simplest approach is to use central differences so that the approximated x and y derivatives of the DEM matrix L at a point identified by the integer indexes (i,j) are:

$$L_x(i,j) = \big(L(i+1,j) - L(i-1,j)\big)/(2\Delta x) \quad \text{and} \quad L_y(i,j) = \big(L(i,j+1) - L(i,j-1)\big)/(2\Delta x) \qquad (1)$$

These expressions correspond to the application of the following filter masks:

$$L_x = \frac{1}{2\Delta x}\begin{bmatrix} 1 & 0 & -1 \end{bmatrix} \cdot L \quad \text{and} \quad L_y = \frac{1}{2\Delta x}\begin{bmatrix} 1 \\ 0 \\ -1 \end{bmatrix} \cdot L \tag{2}$$

where the square brackets identify the two kernels which are convolved with the matrix L to calculate approximations of the derivatives. Since the derivatives have usually higher noise levels than the primitive, the following Sobel kernels (Sobel and Feldman, 1973), which compute the gradient with a degree of smoothing, are preferred:

$$L_x = \frac{1}{8\Delta x}\begin{bmatrix} 1 & 0 & -1 \\ 2 & 0 & -2 \\ 1 & 0 & -1 \end{bmatrix} \cdot L \quad \text{and} \quad L_y = \frac{1}{8\Delta x}\begin{bmatrix} 1 & 2 & 1 \\ 0 & 0 & 0 \\ -1 & -2 & -1 \end{bmatrix} \cdot L \tag{3}$$

3.2. Shaded relief maps

Shaded relief maps are the most common way to represent DEMs, since they show the detail of topographic features in an intuitive manner (e.g. Horn, 1981). Various algorithms are used to calculate hill-shaded maps, most of them depend on the type and number of light sources and on the reflectivity associated with the DEM surface. Users usually find that an oblique illumination from the northwest with a light source shining from a moderate angle between the horizon and zenith, provides the most intuitive images of the shape of the terrain (Kennelly, 2008)

Generally, the hill-shading implemented in GIS software is based on two assumptions: i) the illuminated surface is Lambertian (i.e. it is an ideal diffusely reflecting surface and therefore the apparent brightness of the surface is the same regardless of the observer angle of view); ii) only one light source (usually referred as the sun) is present, at an infinite distance. Hill-shading simulates the diffusion of an artificial light arriving from a single point source at a given altitude (inclination)

and azimuth (declination). Terrain features, irrespective of the angle at which are viewed, have an apparent brightness which is proportional to the cosine of the angle between the normal to the surface and the light-direction vector pointing from the surface to the light source. Supposing the surface to be uniformly white, then the hill-shading gives a typical grayscale image. In the examples of Fig. 2 no active shadow is used. Using an active shadow, even if more realistic, would cast shadow on some areas of the DEM preventing the visualization of any detail in such zones.

As reported by Smith and Clark (2005), shaded relief visualizations are subject to azimuth biasing, altering the position of breaks in slope. As a consequence several features may change shape, appear or disappear (Smith, 2011). In the shaded relief map, the perception of convexity and concavity surfaces depends on the relative location between the viewer and the light source. Changing the direction of illumination to the opposite side, the concavities appear to turn into convexities and vice versa. For example, the lava channels 1 and 2 in Fig. 2b appear to have opposite elevation in Fig. 2c.

The major drawback of shaded relief maps is that linear features, or otherwise features with a certain orientation, may be displayed in a different manner depending on the direction of illumination. This is because ridges and valleys that are oriented perpendicularly to the direction of illumination are much more enhanced than those that are parallel. For example, the terminal part of lava flow 1 is well visible in Fig. 2b and 2e while it is poorly visible in Fig. 2a and 2c. Moreover, the direction of illumination affects the visual perception of the surface roughness in general (Ho et al., 2006).

To avoid a preferential azimuth direction in the lighting some tricks can be used, such as: i) using a single light point source at an elevation angle of 90° (i.e. vertical illumination, see Fig. 2f), in this case for a Lambertian surface the brightness will be proportional to the cosine of the local slope; ii) producing multiple shaded relief images with illumination from multiple directions (Smith and Clark, 2005); iii) producing a single hill-shaded image with more than one light source; and iv) using a non-point source illumination that has no preferential azimuth orientation, such as a uniformly illuminating sky.

In general, after reviewing several visualizations methods, Smith and Clark (2005) and Hillier and Smith (2008) concluded that there is no single visualization techniques that is ideally suited to geomorphological mapping, but the interpreter should prefer techniques that do not introduce azimuth biasing.

3.3. Slope, aspect and curvature maps

Slope, aspect and curvature are here derived directly from the first and the second derivatives of the elevation matrix (e.g. Zevenbergen and Thorne, 1987), calculated by applying Sobel filters (Eq. 3).

The maximum slope (S) is given by definition by:

$$S = \arctan\left[\sqrt{\left(\frac{\partial z}{\partial x}\right)^2 + \left(\frac{\partial z}{\partial y}\right)^2}\right] \tag{4}$$

In the slope map of Fig. 3a, the brightness of each pixel is inversely related to slope angle so that flat areas are bright and steep areas are dark. The resulting image has similar appearance to relief-shaded terrain, without the illumination bias (Smith, 2011). Peaks, pits and passes have zero local slopes. With opportune contrast enhancements (such as applying an area equalization to both of them), slope maps and vertically illuminated hill-shaded models are identical, and both eliminate the azimuth biases typical of obliquely illuminated single-point-source hill-shading (cf. Fig. 2f and 3a).

The aspect angle (θ) is defined as the azimuth direction at which the maximum slope is achieved:

$$\theta = \arctan\left[\left(-\frac{\partial z}{\partial y}\right) \Big/ \left(-\frac{\partial z}{\partial x}\right)\right] \tag{5}$$

Fig. 3d represents the aspect map. Since the aspect corresponds to the azimuthal direction of the gravity force component tangential to the surface, it is said that aspect indicates the flow line direction (Olaya, 2009). Even if the aspect is a circular variable, for sake of simplicity we treat it as a normal variable in the range -180º,+180º.

The overall (local) curvature (C) is defined as the two-dimensional Laplacian $C = \nabla^2 z(x,y)$:

$$C = \frac{\partial^2 z}{\partial x^2} + \frac{\partial^2 z}{\partial y^2} \tag{6}$$

C is positive when the surface is locally concave and negative when the surface is convex. A value of zero indicates that the surface is locally flat. Peaks have negative values of curvature. Pits have positive values of curvature. A curvature map can be used for identifying lineaments on a DEM because it highlights rapid changes at the base and the top of a slope: concave at the base and convex at the summit (Smith and Clark, 2005). When this is calculated across a region, breaks of slope and ridges are well identifiable. For example, the curvature map in Fig. 3b allows easy identification of the scoria cone crater rim and base as well lava channel levees and beds. Fig. 3e shows an example of the multi-curvature (*MC*) parameter calculated as the average curvature at various scales. *MC* retains the same informative content as *C*, but enhances details and the readability of the general topography.

3.4. Topographic position index (TPI) and deviation from mean elevation (DEV) index

Among the various algorithms used to classify landforms (see Hengl and Reuter, 2008 for details), the topographic position index (*TPI*) has become very popular, partly due to its implementation in widespread GIS software. *TPI* is defined as the difference between the elevation

z at a certain point and the average elevation $\bar{z}_R$ around it within a predetermined radius R (Wilson and Gallant, 2000; Reu et al., 2013):

$$TPI = z - \bar{z}_R \tag{7}$$

TPI (Fig. 3c) is a scale-dependent parameter and is used to highlight landscape units such as ridges and valleys on the scale defined by the radius *R*. Positive *TPI* values represent locations that are higher than the average of their surroundings, as defined by the neighborhood (e.g. ridges and peaks, etc.). Negative *TPI* values represent locations that are lower than their surroundings (e.g. valleys and pits). For planar areas, either horizontal or sloping, *TPI* is zero.

Deviation from mean elevation (*DEV*) index is derived by dividing *TPI* by the standard deviation SD_R of the elevations within the radius *R* (Wilson and Gallant, 2000; Reu et al., 2013):

$$DEV = \frac{z - \bar{z}_R}{SD_R} \tag{8}$$

DEV (Fig. 3f) index measures the local deviation from the mean elevation and, like *TPI*, is positive when a point is situated higher than its neighborhood and negative when it is situated lower, but it is mostly restricted to values between –1 and +1 because of its normalization. Values outside this range often indicate anomalies in the DEM. *TPI* and *DEV* are widely used for automatic and semi-automatic landform classification.

3.5. Roughness maps

Surface roughness is an important morphological variable that measures the variability in elevation of a topographic surface at a given scale. The scale of analysis is determined by the size of

the landforms of interest. Several different parameters can be used to quantitatively model surface topographic roughness. One of the most commonly used parameters is the root mean square (*RMS*) height around the mean i.e. the standard deviation of height (e.g. Shepard et al., 2001).

In this work, *RMS* roughness is calculated not around the mean value but as the *RMS* deviation around the interpolating plane (Mazzarini et al., 2008). For each pixel, we consider the local surface defined by a set of DEM points within a predetermined distance *R*. Then we de-trend this surface by subtracting the interpolating plane. Finally, we compute the *RMS* height. By subtracting the interpolating plane the resulting roughness does not depend on the average local slope. This means that the roughness of a plane is always zero, regardless of its inclination. Fig. 4a shows the *RMS* deviation roughness map for the test area.

An alternative approach for computing surface roughness utilizes a different way of measuring the variability in slope and aspect of local patches of a DEM (e.g. Hobson, 1972; Woodcock, 1977; McKean and Roering, 2004). Let's take the surface-normal unit vectors in an $n \times n$ cells sampling window (Fig. 4c). For smooth topography these vectors have coherent orientations while for rough topography their orientations are characterized by a large degree of dispersion. The sums of the cross products of the direction cosines of the surface-normal unit vectors can be organized in a 3 × 3 orientation matrix *T* (Fara and Scheidegger, 1963; Woodcock, 1977):

$$T = \begin{pmatrix} \sum x_i^2 & \sum x_i y_i & \sum x_i z_i \\ \sum x_i y_i & \sum y_i^2 & \sum y_i z_i \\ \sum x_i z_i & \sum y_i z_i & \sum z_i^2 \end{pmatrix} \tag{9}$$

where (x_i, y_i, z_i) are the components of the *N* unit vectors. After calculating the three eigenvalues of this matrix they are ordered from the largest to the smallest, $\lambda_1 \geq \lambda_2 \geq \lambda_3$. Since the sum of the eigenvalues is equal to *N*, the normalized quantities $S_i = \lambda_i/N$, so that $S_1+S_2+S_3 = 1$, can be defined. Because of the normalization, there are only two independent quantities S_i. S_i describes the amount and nature of clustering of the vector orientations: the ratio S_1/S_2 is defined as flatness and the ratio

S_2/S_3 is called organization (Coblentz and Karlstrom, 2011). These ratio values are often not normally distributed, hence it is more convenient to use their logarithms (Fig. 4c, d). The ratio of $\ln(S_1/S_2)$ to $\ln(S_2/S_3)$ was defined as the *K*-value by Woodcock (1977) and can be used to evaluate the clustering of the normal vector distribution.

Hobson (1972) measured the surface roughness as $1/N$ times the length of the vector sum of all the unit vectors in the moving window of Fig. 4c:

$$R = \frac{1}{N}\sqrt{\left(\sum x_i\right)^2 + \left(\sum y_i\right)^2 + \left(\sum z_i\right)^2} \tag{10}$$

where (x_i, y_i, z_i) are again the components of the N unit vectors. If the surface is perfectly flat the vector sum is a vector with a length equal to N so that $R = 1$. The rougher the surface, the lower the length of the vector sum (Fig. 4d). The unconsolidated deposits of a scoria cone, most of which are cinder-sized, have low roughness, while lava channels have high roughness (Fig. 4).

3.6. Sky view factor

Preferential directions due to the lighting in hill-shading (see Fig. 2) can be also avoided by using uniform diffuse illumination instead of point light sources. Supposing that the entire celestial hemisphere is equally bright, the illumination of a given point on a DEM is proportional to the portion of the sky that is visible from the point itself. The portion of visible sky is a measurable physical quantity (Fig. 5) and is called Sky View Factor (*SVF*; Steyn, 1980). *SVF* is given by the ratio of the solid angle of the visible sky (Ω_{sky}) to the solid angle of the illuminating hemisphere (= 2π):

$$SVF = \frac{W_{sky}}{2\pi} \tag{11}$$

The end members *SVF* = 0 and *SVF* = 1 mean that no portion of the hemisphere and the entire hemisphere are visible from the taken point, respectively. Calculating *SVF* at each point of a DEM is very CPU consuming. Therefore the first step to speed up calculations is to introduce a maximum search radius *R* within which possible obstacles that may mask portions of the sky are considered. Then, *SVF* is usually approximated by considering the "openness" to the sky along a number of directions (*n*) instead of doing the complete calculation (Fig. 5 and Zakšek et al., 2011):

$$SVF = 1 - \frac{1}{n}\sum_{i=1}^{n} \sin \gamma_i \tag{12}$$

where γ_i is the elevation angle of the visible horizon. In Eq. 12 γ_i cannot be negative to limit the estimation of each elevation angle by the mathematical horizon (Zakšek et al., 2011). If we allow γ_i to take negative values in Eq. 12, we obtain a new quantity that can reach a maximum possible value of 2 (here called *SVF*2).

Uniform diffuse sky illumination of *SVF* and *SVF*2 not only solves the problems of feature orientation but also enhances the perception of the relative height of surface elements (Fig. 6a, b). In general *SVF* and *SVF*2 display very similar behavior, although they have significantly different values along sloping planes. This difference can be appreciated by comparing the flanks of the scoria cone in Fig. 6a and 6b.

SVF only deals with the ridges of the topography. To introduce a similar quantity that deals with the depressions, first we mirror our surface $z=f(x,y)$ across a horizontal plane obtaining a new surface $z=g(x,y)$ with $g(x,y)= -f(x,y)$. Then we calculate the SVF of this inverted surface $z=g(x,y)$ and we call this new quantity "mirrored *SVF*" (Fig. 6c). SVF takes high values on crests and ridges while the "mirrored *SVF*" takes high values inside valleys, gullies and craters (Fig. 6a, c).

3.7. Openness maps

Yokoyama et al. (2002) introduced two parameters called positive and negative openness. The positive openness is defined as:

$$\Phi_R = \frac{1}{n}\sum_{i=1}^{n}\phi_i = 90° - \frac{1}{n}\sum_{i=1}^{n}\gamma_i \tag{13}$$

where ϕ_i is the zenith angle along the *i*-th direction and γ_i are defined as in Equation 12 but here are not limited to be positive (Fig. 5). The subscript *R* refers to the maximum horizontal search radius considered. Similarly the negative openness is defined as:

$$\Psi_R = 90° - \frac{1}{n}\sum_{i=1}^{n}\psi_i \tag{14}$$

where ψ_i is defined in Fig. 5c. Both positive (or openness up) and negative (or openness down) openness always take positive values. The former measures the "openness of the terrain to the sky" while the latter is the "below-ground" openness (Yokoyama et al., 2002). The positive openness takes high values on crests and ridges; the negative openness takes high values inside valleys, gullies and craters (Fig. 6e, f).

Later Chiba et al. (2008) introduced a new parameter, generically called mere "openness", combined from the positive and negative openness as:

$$Openness = \frac{1}{2}(\Phi_R - \Psi_R) \tag{15}$$

The openness is dependent on the chosen search radius *R* and is positive when the surface, at the scale *R*, is upwardly convex (i.e. crests and ridges) and negative when the surface is upwardly concave (i.e. in valleys, gullies and craters; Fig. 6d).

4. Image combination

Image combination may be defined as the combination of two or more images representing different parameters. The aim is to obtain a new colored hybrid image containing and representing more information than the individual original images (Fig. 7). Generically, image composition improves the image quality by enhancing the investigated details during the visual analysis. Image composition can be obtained following various techniques.

Widespread and useful maps derived using image composition are, for example, colored layer draped on hill-shaded images, which are often created with geographic information systems (GIS) using the Hue–Saturation–Value (HSV) color model. HSV is a common cylindrical-coordinate representation of points in an RGB color mode where *H* is hue, *S* is saturation, and *V* is value. The hue of a generic point in the color space is its pure color; for example, all tints, tones and shades of red have the same hue. The saturation defines how pure a color is by giving its degree of degradation into gray tones: a pure color has a 100% saturation, and 0% saturation means that the color has completely lost its "color" and is only a shade of gray. The value, also called lightness, defines how dark a color is: a pure color has a 100% value and a value of 0 is black.

The most basic image composition for enhancing topographic details is overlaying a colored thematic map (the hue dimension in the HSV space) to a hill-shaded map (that is the SV color space dimensions). For example, a map color-coded according to pixels' elevations or color-coded according to the thickness of a new emplaced lava flow can be overlaid to a hill-shaded map as shown in Fig. 7a.

Using HSV color fusion technique, Chiba et al. (2008) developed the "Red Relief Image Map" (RRIM). They fix the hue to be red, thus producing a red image by adjusting the saturation value of red based on the topographic slope and its lightness (or value) based on the openness (Fig. 7b and 7c). It accentuates the three-dimensional topography on a single image, where the openness value virtually performs an illumination role, and saturation of red color describes the steepness of topography. Karátson et al. (2016) used the RRIM for visualizing at the same time slope, concavity and convexity from the DEM of Gran Canaria Island. The authors chose RRIM because it effectively represents fine geomorphic features even on a largely flat surface and used it for successfully extracting planèzes and quasi-planar surfaces.

The reason for the use of red color in the RRIM is that it proved empirically to have the richest tone for human eyes, although other colors can also be applied (Chiba et al., 2008). A generic map can also be used to assign different hues to every pixel according to the thematic map values. Fig. 7d shows an example of RRIM in which hues are assigned as a function of the thickness of lava flows emplaced between 2005 and 2007.

"RRIM style" maps (that is more generic HSV compositions) can be produced by changing the starting maps used by Chiba et al. (2008). In order to best exploit the potential of RRIM it would be wise to use starting maps bearing completely different information. For example, in Fig. 7e the *SVF*2 and slope are used as saturation and value respectively. Although SFV2 and openness maps are very similar (compare Fig. 6b with Fig. 6d), swapping *SVF*2 with the slope in the "RRIM style" image completely changes the visual effect of the composition.

Beside manipulations in the HSV color space, other image compositions can be used. For example, in Fig. 7f we enhanced the slope by adding the roughness (a de-trended *RMS* deviation in this case). In this new map the areas with rapid changes in slope (which have high roughness) are very bright and very accurately delimit areas with similar values of slope. As a result, this map emphasizes, for example, the external levee walls of lava flows.

5. Surface parameter comparison

Surface parameters are, in many cases, correlated with one another. For example, a hill-shaded map with 90° of sun elevation angle and a slope map are very similar (cf. Fig. 2f and 3a), as well as curvature maps and *TPI* and *DEV* maps (cf. Fig. 3b, c and f), and *SVF* maps and openness up maps (cf. Fig. 6b and e). Taking into account that the amount of data can be very large, knowing *a priori* how to use the computing resources is very useful for minimizing computing time. Distinguishing between correlated and uncorrelated parameters allows the operator to choose which maps should be produced from a DEM and which are instead unnecessary.

In this section, we compare surface parameters with one another by creating a correlation matrix.

Given two grids, *A* and *B*, we use the covariance between them to measure how similarly the two grids vary in space:

$$COV\ (A,B) = \frac{1}{n-1}\sum_{i,j}(a_{ij}-\bar{a})(b_{ij}-\bar{b}) \tag{16}$$

where a_{ij} and b_{ij} are the grid values of *A* and *B*, respectively, in the cell of position *i*,*j*. The sum on *i*,*j* spans all *n* cells of the grids. A positive value of the covariance means that the two grids tend to have a similar behavior: greater values of the first grid mainly correspond to greater values of the second, etc. On the other hand, a negative value of the covariance means that the two grids tend to have opposite behavior: greater values of the first grid mainly correspond to smaller values of the second grid and *vice versa*. The magnitude of the covariance depends on the variability of both grids. For this reason we prefer to normalize the covariance by dividing it by the product of the corrected standard deviations of the two grids, S_A and S_B:

$$S_A = \sqrt{\frac{1}{n-1}\sum_{i,j}(a_{ij}-\bar{a})^2} \quad \text{and} \quad S_B = \sqrt{\frac{1}{n-1}\sum_{i,j}(b_{ij}-\bar{b})^2} \tag{17}$$

to obtain a normalized version of the covariance better known as the correlation coefficient:

$$COR(A,B) = \frac{COV(A,B)}{S_A S_B} = \frac{\sum_{i,j}(a_{ij}-\bar{a})(b_{ij}-\bar{b})}{\sqrt{\sum_{i,j}(a_{ij}-\bar{a})^2 \sum_{i,j}(b_{ij}-\bar{b})^2}} \tag{18}$$

The correlation coefficient ranges between -1 and +1. A correlation of +1 means that there is a perfect direct linear relationship between the two grids and a correlation of -1 means that there is a perfect negative linear relationship between the two grids. In any case, for both +1 or -1 correlations, the two quantities are in a perfect linear relationship. Since for practical comparison we are more interested in the magnitude of correlation rather than the sign, we prefer to consider squared correlation values, so a value of 1 means that the two grids are perfectly correlated either directly or inversely. As the squared correlation approaches 0 (from 1), the two quantities are less and less correlated up to the point that for a value of 0 there is no correlation between the spatial trends of the values of the two grids.

Fig. 8 shows the squared correlation matrix among the reviewed parameters in the test case area described above. Fig. 9 shows the square correlation matrix among the reviewed parameters calculated for four different DEMs of four areas with heterogeneous topography: i) the 1-m LIDAR DEM test area of this work; ii) the 10-m resolution 2005 DEM of Etna region (Italy) produced by merging of a 1-m LIDAR DEM (Favalli et al., 2009) and TINITALY DEM (Tarquini et al., 2012); iii) the 10-m resolution DEM of Tenerife Island (Canary Islands, Spain) produced by GRAFCAN (2009); and vi) the SRTM DEM (http://www2.jpl.nasa.gov/srtm), resampled to 120 m, of a region of the Blue Nile river basin (Ethiopia).

Fig. 8 and 9 show that the chosen DEMs provide very similar results that can be summarized as follows. Hill-shaded maps are not or poorly correlated with the other parameters. Only hill-shaded maps computed with a sun elevation angle of 90° are well correlated with slope maps and variously

correlated with *SVF* maps. Hill-shaded maps computed from opposite azimuths contain very similar information. Slope is largely uncorrelated except for certain correlation with *SVF*. The curvature parameters are generally somewhat correlated with *SVF* and openness parameters. Roughness is uncorrelated with the curvature parameters and very poorly correlated with the hill-shading. Openness up is well correlated with *SVF* parameters, while openness down is not.

On the whole, in order to have the most uncorrelated content the following maps should be produced: various hillshading, slope, a curvature map, a *TPI* map with high R, 3 roughness maps, openness down, openness and one of a choice between *SVF*, *SVF*2 and openness up. Uncorrelated parameters can be combined in order to obtain a more informative map. In the following case studies, the surface parameters and their representations were chosen after taking into account the features we want to detect and avoiding redundant information.

6. Case studies

6.1 Michoacán-Guanajuato volcanic field

Morphometric analysis of complex volcanic fields benefits from the large availability of various DEMs (e.g. Favalli et al., 2009; Fornaciai et al., 2012): however delineating their basic elements can be difficult. These areas are characterized by the frequent superimposing of lava flows that often bury the base of edifices, by chains of eruptive vents that generate coalescent cones and volcanoes, and by huge fallout of ash that drapes all features.

The Michoacán-Guanajuato Volcanic Field in central Mexico contains over 1000 late Quaternary volcanic centers, of which approximately 90% are cinder cones (Hasenaka and Carmichael, 1985). The highest resolution free DEM of this area is the 30 meter ASTER GDEM (Fig. 10a). The hill-shaded image (Fig 10a and b) shows the complexity of this volcanic area, which is characterized by a large number of scattered cinder cones and shield volcanoes, lava domes,

maars and lava flows. Although it can be quite simple to just mark each volcanic center, outlining their bases can be demanding because several of them are in close proximity to each other. The openness down map is able to enhance even barely visible depressions, such as those between contiguous volcanic edifices and thus it can be used for detecting the base of the cones: in Fig. 10c the flanks of the volcanoes are represented by bright tones (low openness down values), while the incisions between an edifice and its neighbors are dark (high openness down values). The benefit in using openness down is shown in the insets of Fig. 10c, where we compare the hill-shaded and the openness down maps of a selected cone. The delimitation of its base is largely left to the interpretation of the operator using the hill-shading while the openness map turns out to be more informative.

The hill-shading and openness maps alone are not enough to resolve the complex topography of this area. Other parameters are required in order to reveal different details and facilitate the recognition of various-scale objects, possibly avoiding bearing the same information as the already calculated maps. In this case, we use the "RRIM style" map composed with the slope and the *SVF*. Fig. 10d shows how this map can be tuned for resolving topography. Crater rims are outlined as bright lines and can therefore be easily mapped. On the contrary, craters and gullies of ancient volcanic edifices stand out as dark regions. In particular, the craters are visible as small, dark, and roundish areas of lower map values. Since this map gives a much better impression on the relative elevation of each point, the lava flow of the inset of Fig. 10d, taken as an example, is more visible than in the hill-shading. In addition, it is also possible to see all the small ridges in a relatively flat relief such as the scarp and hydrographic network southeast to the Pico Tancitaro. Semi- or completely automatic methods for cone delineation, based on primary DEM derivatives such as slope angle or curvature maps, had already been used (e.g. Grosse et al. 2012; Karátson et al. 2012).

6.2 Roques Blancos phonolitic lava flow

Morphometry of lava channels is important in understanding the emplacement processes operating during effusive eruptions (Tarquini et al., 2012; Lev and James, 2013). Dimensional and morphometric features of lava channels are not easy to measure. Field methods that yield such data are difficult and time consuming to apply due to the difficult nature of the terrain. Moreover, visual interpretation of data collected by remote instruments can be difficult because of the superimposing of various flows often during the same eruption.

Fig. 11 shows hill-shaded, openness and *SVF* maps of a Roques Blancos phonolitic lava flow field, NW of the Pico Viejo stratocone (Tenerife Island). The Roques Blancos lava flow was erupted about 1714 BP from a dome located at an elevation of 2700 m a.s.l. (Carracedo et al., 2007).

The shaded relief (Fig 11a) shows a general topography composed of a complex system of ramified channels characterized by thick flows, steep fronts and conspicuous levees. However, channels running from NW to SE are not well visible because they are aligned with the illumination direction. Already Smith and Clark (2005) made analyst aware that the use of a directional light source introduce bias especially in case of linear landforms. It is quite obvious that this problem is particular relevant in mapping lava flow. All linear features are instead clearly visible in both *SVF* and openness down images (Fig 11b and c), which allow untangling this complex system of channels. The *SVF* map depicts the empty channel in distinct dark tones, which makes them easily identifiable and the levee ridges are outlined as bright lines and can therefore be easily mapped (Fig. 11a, b, dashed lines). The openness down map reveals additional important information: while the rims of levees are less pronounced, their deepest parts are clearly marked. Also, the lobate forms of the lava front, composed by curved superimposed layers, are properly visualized. Finally, the openness down map gives a clear idea of the considerable thickness of these phonolitic lavas.

These maps can be used for extracting the interesting features in a semi-automatic way. From a practical point of view, even if the *SVF* fruitfully identifies the levee rims, their automatic extraction using this map is troublesome and indeed it is much more simply performed by

extracting these lines as portions of contour lines of the hill-shaded map of Fig. 11a. In fact the levee rims identify the points where the shading changes from low to high values (opposite sides of the levee). Similarly, by choosing the proper value of openness down, the contour line of the lava flow can be extracted and used for calculating the lava extension, length and volume. The same procedure can be done for extracting the edge of the channel bed. In the example of Fig. 11c, the values of 86º and 81.5º for the openness down map can be used for automatically delineating the isolines that best delimit the base of the lava and the bed of the channel, respectively. After very minor editing operations, consisting mainly of cutting out unwanted part of the isolines, the shapefiles of the base and the bed of the lava channel are extracted (Fig. 11).

7. Discussion

The growth of new remote sensing technologies capable of producing topographic data with high accuracy at reasonable costs, and the availability of web-shared DEMs, offer great opportunities to better map and quantify features in volcanic areas. In order to make the best use of the great availability of these large amounts of data it is necessary to know what information can be extracted from a DEM and how to effectively use the computing resources.

The most used DEM representation for mapping and measuring volcanic features is the shaded relief map. It is very informative and provides an immediate picture of the 3D distribution of landforms. Hill-shading maps generated using an oblique illumination with a light source shining from a moderate angle between the horizon and zenith, and from the northwest, provide the most intuitive images of the shape of the terrain. An active shadow would give a more realistic representation of the terrain, but at the same time would cast shadow on some areas of the DEM preventing the visualization of any detail in such zones. The major drawback of using hill-shaded map the is done by the fact that the angle of illumination, or azimuth, strongly affects the way features appear. In other words in the hill-shaded map the perception of the convexity and concavity

of surfaces depends on the relative position of the light source (Fig. 2). As a consequence, features with a certain orientation may be displayed in a different manner depending on the direction of illumination or, even worse, they can be in the shadow and not visible at all. In addition linear features, or otherwise features with a certain orientation, may be displayed in a different manner depending on the direction of illumination. For these reason, if only hill-shading maps are available, it is recommended to compare maps produced with different directions of illumination. For a Lambertian surface, hill-shading with an elevation angle of 90° yields a brightness proportional to the cosine of the local slope thus it is just a reclassification of a slope map (cf. Fig. 2f and Fig 3a).

Besides hill-shaded maps, the slope (Fig. 3a), the aspect (Fig 3d), the *SVF* (Fig 6a-c) and the openness (Fig 6d-f) as well as RRIM maps (Fig. 8) are enough to present and describe, by themselves, the topography and morphological characteristics. They all act like hill-shading so they can be used to visualize a DEM, although each of them highlights particular aspects of the relief. Slope maps and vertically illuminated hill-shaded models are, by properly adjusting the contrast, very similar or identical. Both of them eliminate the azimuth biases typical of obliquely illuminated single-point-source hill-shading. It follows that slope maps can be used instead of hill-shaded maps to overcome some drawbacks. The aspect map, with appropriate gray scale color legend, is very similar to a hill-shaded map (e.g. Fig. 3d); the legend can be easily changed in order to mimic a different azimuthal direction of illumination. The *SVF* maps are actually just a different kind of hill-shading with a uniform diffuse illumination (Fig. 5) and the openness up maps are very similar in construction to the *SVF* maps and then by definition very similar to *SVF*, that is in the limit of small angles. In particular, it is evident that openness up and *SVF*2 produce very similar maps when we convert the grids into images (cfr. Fig. 6b and 6e). This is because in the approximation of small angles results in $\sin(\gamma_i) = \gamma_i$ (with angles expressed in radians). As a consequence the openness up and *SVF*2 maps only differ in areas where we have big angles γ_i. For example, the test area in Fig. 6, which contains several steep structures and has a very high roughness (see Fig. 4), has an average openness up angle of 81° so that the average γ_i value is 9°, that is 0.1571 in radians, while its sine is 0.1564 and so, on average, γ_i and $\sin \gamma_i$ differ only by 0.4 %. *SVF* differs from *SVF*2 (and thus also

from openness up) mainly on ridges and on slopes with horizontal dimensions greater than the search radius *R* (e.g. the slopes of the scoria cone in Fig. 6a,b and e). Analogously the mirrored *SVF* and the openness down mainly differ in the pits and valleys and again on slopes with horizontal dimensions greater than *R* (cfr. Fig. 6c and 6f).

The curvature (Fig. 3b) looks like an edge detection filter (as it actually is). The multi-curvature map (Fig. 3f), collecting contributions of curvatures at very different length scales, provides an alternative way to put in evidence the various shapes; it looks more like a morphological filter and is very well correlated with openness. *TPI* and *DEV* are very similar and not visually very expressive (Fig. 3c, f). They are generally used for automatic classification of land features. The roughness map describes how complex the terrain is and so, it is a standalone and crucial parameter.

Color images are important because human eyes are sensitive to thousands of color shades which helps us in object identification. In addition, a color image can be composed by different grey-tone images, with each of them retaining different information. In the authors' opinion the best single image technique that is devoid of azimuth-bias and yet portrays the landscape optimally is, so far, the Red Relief Image map introduced by Chiba et al. (2008). It does not have a preferential direction (unlike classical hillshading) and, moreover, it is more readable if compared to images composed using *SVF* or openness up, where local depressions are in the dark and much data is missing. On the other hand, ridges are much better defined and identified using *SVF* or openness up, and valleys and depressions by using openness down or inverted *SVF*.

By simply analyzing the visual representation of parameters described above, it is clear that many of them contain almost the same information or that they are practically the same map. The correlation matrices (Fig. 8 and 9) produced in this work were obtained by calculating the correlation coefficient among each couple of analyzed parameters for four DEMs with various sources and resolutions. These matrices are a useful starting point for defining which parameter combinations can provide key information of the terrain and which of them are instead redundant. In the same way, the correlation matrix can be used to aid in the choice of map combinations for

possible HSV colored maps. It is indeed obvious that to create an HSV map starting from images containing the same information is pointless.

Some of the relevant information that can be extracted from the correlation matrix is described in the following. First, we should note that in general the correlation between parameters shows slightly to no changes when using DEMs from different sources and with different resolution. Sometimes these differences can be more relevant. This can be due to the difference in DEM resolution or to differences in the terrain characteristics. A DEM is the most uncorrelated map, but, of course, it cannot be visually analyzed without further elaborations. Hill-shading maps are widely uncorrelated with all the other parameters. Only hill-shaded maps calculated using a vertical illumination are correlated with the slope and, somehow, with *SVF* maps. It should be noticed that inside the "hill-shaded" group the correlation depends on the illumination angles; in particular hill-shaded maps with opposite azimuthal angles of illumination are strongly correlated. Also, the aspect is basically uncorrelated with all the examined parameters, except for some correlation with the hill-shaded maps. This is consistent with the results obtained by Evans and Cox (1999) who inter-compared zero, first and second derivatives of elevation. In addition to the vertical illuminated hill-shading, the slope has some correlation only with the *SVF* maps, but this seems to be dependent on the DEM source. In agreement with Evans and Cox (1999), slope is poorly correlated with DEM and curvature. The "curvatures" group contains heterogeneous parameters. They have almost no correlation with any type of hillshading and with slope and aspect, as also showed by Evans and Cox (1999). In general, they have some correlation with the openness group (especially with multi-curvature) maps and, to a minor extent, with the *SVF* group. Curvature and multi-curvature are correlated with both openness up and down but there are some differences depending on the DEM source. As expected, *TPI* 2pix and curvature are highly correlated since they are calculated in almost the same way; on the contrary, *TPI* 100 pix and curvature are not correlated. *TPI* and *DEV* maps are correlated only if they are calculated over windows with the same size. Overall roughness parameters are only correlated with other roughness parameters. Openness up is well correlated with *SVF* maps, however, openness down is not. Openness 20 pix and multi-curvature are highly

correlated. Inside the "openness" maps we notice that openness down is uncorrelated to openness up. Openness parameters are uncorrelated with hill-shading and roughness. *SVF* is somehow correlated with the slope. *SVF*2 is independent on the slope but it is correlated with the curvature. In particular, *SVF*2 with a searching radius of 20 pix is highly correlated with the multi-curvature.

The increasing availability of various DEMs at different resolutions and coverage has been giving new research opportunities for volcano geomorphology studies. Detecting and delineating features in volcanic areas can be everything but easy because of their extreme complexities: volcanic areas are characterized, for example, by the superimposing of lava flows, coalescent cones and volcanoes, huge ash fallout and, last but not least, if active, they are often dramatically changed by new eruptions. For this reason it can be very useful to have informative maps which enhance specific volcanic landforms. For example, in the Michoacán-Guanajuato volcanic field the base of the cones can be easily detected by using the openness down map despite the difficulties arising from the large number of superimposed features. In the same way, *SVF* and openness down images allow the complex system of channels of the Roques Blancos phonolitic lava flow to be untangled, enabling detection of levees, the base and the bed of the channels. These parameters can be used for performing a semi-automatic extraction of the main landform elements, helping to make the job of the analyst quick and precise.

8. Conclusion

Digital Elevation Models permit the extraction of many different parameters, starting from a single matrix of elevation values. In this work we describe a series of DEM-derived parameters focusing on their benefit for enhancing specific land features. The main relevant results and outcomes obtained from this work and by reviewing the previous studies are:

- In converting a grid to an image, the 2.5σ equalization, in general, is a suitable compromise between the image enhancement and the necessity to keep the shape of its histogram.

- Slope and *SVF* (or openness map) can be combined in RRIM "style" maps in order to bear in one single colored image all benefits contained in each of the single starting images.
- In addition to common and less common parameters, in this work we introduce and represent the following parameters: *SVF*2 (Fig. 6b), the Mirrored *SVF* (Fig. 6c), plus other map combinations as presented in the Fig. 7c, e and f.
- Uniform diffuse sky illumination of *SVF* and *SVF*2 is actually hill-shading but it eliminates the azimuth biases and also enhances the perception of the relative height of surface elements.

Several DEM-derived parameters can have similar or almost the same informative content, and consequently one or more parameters can be redundant. In this work, we produce a correlation matrix for rapidly detecting which parameters are correlated and which are not. This matrix helps to: i) choose which parameters should be used in image combinations, since by composing the uncorrelated parameters we can obtain a more informative map; and ii) save computational resources avoiding calculation of parameters containing the same information.

The most noteworthy conclusions that can be summarized from the correlation matrix are:

- Hill-shading, aspect and roughness maps are poorly or un-correlated with all the parameters.
- Only hill-shaded maps computed with a sun elevation angle of 90° are well correlated with the slope map and variously correlated with *SVF* maps.
- Hill-shaded maps computed from opposite azimuths contain very similar information.
- Slope is largely uncorrelated except for some correlation with the *SVF* group.
- The curvature parameters are generally somewhat correlated with *SVF* and openness parameters.
- Openness up is well correlated with *SVF* parameters, unlike openness down.
- In order to have the most uncorrelated content from a DEM, the following parameters should be produced: various hill-shading, slope, a curvature, a *TPI* with high R, roughness, negative openness, openness and one of choice among *SVF*, *SVF*2 and openness up.

Finally, the dissertation of this work and the correlation matrix represent a useful tool for analyzing morphologies in volcanic areas. For example, features such as the bases of a volcanic edifice and the base of lava channels, characterized by a particular slope break, can be easily detected and semi-automatically extracted by using the openness down map. Otherwise *SVF*, either alone or combined in RRIM, is very useful for distinguishing volcanic features that are slightly raised relative to their surroundings, since it enhances the perception of the relative height of surface elements. In addition, since *SVF* takes high values on crests and ridges, it helps to detect and map the levees of lava channels and to distinguish among superimposed channels.

Acknowledgements. Authors are grateful to Hannah Reynolds for reviewing English style and grammar and to Andrea Agostini for the critically reading the manuscript. We especially thank Paolo Tarolli and Ian S. Evans for detailed and constructive reviews that greatly improved the manuscript. Editorial handling by Takashi Oguchi is much appreciated. AF has carried out this work in the frame of Dottorato di Geofisica, Dipartimento di Fisica e Astronomia, University of Bologna.

References

Buckley, A., Hurni, L., Kriz, K., Patterson, T., Olsenholler, J., 2004. Cartography and visualization in mountain geomorphology. Geographic Information Science and Mountain Geomorphology. Springer, Praxis, Chichester, UK, 253-287.

Carracedo, J.C., Rodríguez Badiola, E., Guillou, H., Paterne, M., Scaillet, S., Pérez Torrado, F.J., Paris, R., Fra-Paleo, U., Hansen, A., 2007. Eruptive and structural history of Teide Volcano and rift zones of Tenerife, Canary Islands. Geol. Soc. Amer. Bull. 119 (9), 1027–1051. doi:10.1130/B26087.1.

Cayley, A., 1859. On Contour Lines and Slope Lines. Philosophical Magazine: A Journal of Theoretical, Experimental and Applied Physics 18, 264-268.

Chiba, T., Kaneta, S. I., Suzuki, Y., 2008. Red relief image map: new visualization method for three dimensional data. The International Archives of the Photogrammetry. Remote Sensing and Spatial Information Sciences 37, 1071-1076.

Coblentz, D., Karlstrom, K. E., 2011. Tectonic geomorphometrics of the western United States: Speculations on the surface expression of upper mantle processes. Geochemistry, Geophysics, Geosystems 12(11).

De Reu, J., Bourgeois, J., Bats, M., Zwertvaegher, A., Gelorini, V., De Smedt, P., Chu, W., Antrop, M., De Maeyer, P., Finke, P., Van Meirvenne, M., Verniers, J., Crombé, P., 2013. Application of the topographic position index to heterogeneous landscapes. Geomorphology 186, 39 –49.

Evans, I.S., Cox, N.J., 1999. Relations between land surface properties: altitude, slope and curvature. In: Hergarten, S., Neugebauer, H.J. (Eds.), Process Modelling and Landform Evolution. Springer, Berlin, pp. 13–45.

Fara, H. D., Scheidegger, A. E., 1963. An eigenvalue method for the statistical evaluation of fault plane solutions of earthquakes. Bulletin of the Seismological Society of America 53(4), 811-816.

Favalli, M., Fornaciai, A., Pareschi, M.T., 2009. Lidar strip adjustment: application to volcanic areas. Geomorphology 111, 123–135.

Favalli, M., Fornaciai, A., Isola, I., Tarquini, S., Nannipieri, L., 2012. Multiview 3D reconstruction in geosciences. Comput. Geosci. 44, 168–176.

Fisher, N. I., Lewis, T., Embleton, B. J., 1987. Statistical analysis of spherical data. Cambridge University Press, U.K., pp. 329.

Fornaciai, A., Favalli, M., Karátson, D., Tarquini, S., Boschi, E., 2012. Morphometry of scoria cones, and their relation to geodynamic setting: a DEM-based analysis. J. Volcanol. Geotherm. Res. 217/218, 56–72.

GRAFCAN, 2009. Mapa Topográfico de las Islas Canarias (1:5.000). Cartográfica de Canarias, Spain.

Grosse, P., van Wyk de Vries, B., Euillades, P.A., Kervyn, M., Petrinovic, I.A., 2012. Systematic morphometric characterization of volcanic edifices using digital elevation models. Geomorphology 136, 114–131.

Hasenaka, T., Carmichael, I.S.E., 1985. The cinder cones of Michoacán–Guanajuato, Central Mexico: their age, volume and distribution, and magma discharge rate. Journal of Volcanology and Geothermal Research 25, 105–124.

Hengl, T., Evans, I.S., 2009. Mathematical and digital models of the land surface. In: Hengl, T., Reuter, H.I. (Eds.), Geomorphometry: Concepts, Software, Applications. Elsevier, Amsterdam, pp. 31–63.

Hengl, T., Reuter, H.I. (Eds.), 2009. Geomorphometry: Concepts, Software, Applications. Elsevier, Amsterdam.

Hiller, J.K., Smith, M., 2008. Residual relief separation: digital elevation model enhancement for geomorphological mapping. Earth Surf. Process. Landf. 33, 2266–2276.

Ho, Y. X., Landy, M. S., Maloney, L. T., 2006. How direction of illumination affects visually perceived surface roughness. Journal of Vision 6(5), 634–648.

Hobson, R.D., 1972. Surface roughness in topography: a quantitative approach. In R.J. Chorley (Ed.), Spatial Analysis in Geomorphology, Methuen & Co, London, pp. 221–245.

Horn, B.K.P., 1981. Hill shading and the reflectance map. Proc. IEEE 69 (1), 14–47.

James, M.R., Robson, S., 2012. Straightforward reconstruction of 3D surfaces and topography with a camera: accuracy and geoscience application. Journal of Geophysical Research — Earth Surface 117, F03017. http://dx.doi.org/10.1029/2011JF002289.

Karátson, D., Telbisz, T., Wörner, G., 2012. Erosion rates and erosion patterns of Neogene to Quaternary stratovolcanoes in the Western Cordillera of the Central Andes: an SRTM DEM based analysis. Geomorphology 139, 122–135.

Karátson, D., Yepes, J., Favalli, M., Rodríguez-Peces, M. J., Fornaciai, A., 2016. Reconstructing eroded paleovolcanoes on Gran Canaria, Canary Islands, using advanced geomorphometry. Geomorphology 253, 123-134.

Kennelly, P. J., 2008. Terrain maps displaying hill-shading with curvature. Geomorphology, 102(3), 567-577.

Kolzenburg, S., Favalli, M., Fornaciai, A., Isola, I., Harris, A.J.L., Nannipieri, L., Giordano, D., 2016. Rapid updating and improvement of airborne LIDAR DEMs through ground based SfM 3D modeling of volcanic features. IEEE Transactions on Geoscience and Remote Sensing PP (99), 1-13.

Lev, E., James, M.R., 2014. The influence of cross-sectional channel geometry on rheology and flux estimates for active lava flows. Bull. Volcanol. 76(7), 1-15.

Mazzarini, F., Favalli, M., Isola, I., Neri, M., Pareschi, M.T., 2008. Surface roughness of pyroclastic deposits at Mt. Etna by 3D laser scanning. Annals of Geophysics 51(5-6), 813-822.

McKean, J., Roering, J., 2004. Objective landslide detection and surface morphology mapping using high-resolution airborne laser altimetry. Geomorphology 57(3), 331-351.

Mitasova, H., Harmon, R. S., Weaver, K. J., Lyons, N. J., Overton, M. F., 2012. Scientific visualization of landscapes and landforms. Geomorphology 137(1), 122-137.

Olaya, V., 2009. Basic land-surface parameters. In: Hengl, T., Reuter, H.I. (Eds.), Geomorphometry: Concepts, Software, Applications. Elsevier, Amsterdam, pp. 141–169.

Shepard, M.K., Campbell, B.A., Bulmer, M.H., Farr, T.G., Gaddis, L.R., Plaut, J.J., 2001. The roughness of natural terrain: a planetary and remote sensing perspective. Journal of Geophysical Research 106, 32,777–32,795.

Smith, M.J., Clark, C.D., 2005. Methods for the visualisation of digital elevation models for landform mapping. Earth Surface Processes and Landforms 30, 885–900.

Smith, M.J., 2011. Chapter eight – digital mapping: visualisation, interpretation and quantification of landforms. In: Smith, M.J., Paron, P., James, S.G. (Eds.), Developments in Earth Surface Processes. Elsevier, Amsterdam, pp. 225–251.

Sobel, I., Feldman, G., 1973. A 3 × 3 Isotropic Gradient Operator for Image Processing. In Duda, R., Hart, P., (Eds.), Pattern Classification and Scene Analysis. Wiley , New York, pp. 271–272.

Steyn, D., 1980. The calculation of view factors from fisheye-lens photographs. Atmos. Ocean 18, 254-258.

Tarolli, P., 2014. High-resolution topography for understanding Earth surface processes: opportunities and challenges. Geomorphology 216, 295 –312.

Tarquini, S., Vinci, S., Favalli, M., Doumaz, F., Fornaciai, A., Nannipieri, L., 2012. Release of a 10-m-resolution DEM for the Italian territory: Comparison with global-coverage DEMs and anaglyph-mode exploration via the web. Computers and Geosciences 38(1), 168–170.

Tarquini, S., Favalli, M., Mazzarini, F., Isola, I., Fornaciai, A., 2012. Morphometric analysis of lava flow units: case study of lidar-derived topography at Mount Etna, Italy. J. Volcanol. Geotherm. Res. 235–236, 11–22.

Westoby, M.J., Brasington, J., Glasser, N.F., Hambrey, M.J., Reynolds, J.M., 2012. 'Structure-from-Motion' photogrammetry: a low-cost, effective tool for geoscience applications. Geomorphology 179, 300–314.

Wilson, J.P., 2012. Digital terrain modeling. Geomorphology 137, 107–121.

Wilson, J.P., Gallant, J. C. (Eds.), 2000. Terrain analysis: principles and applications. Wiley.

Woodcock, N. H., 1977. Specification of fabric shapes using an eigenvalue method. Geological Society of America Bulletin 88(9), 1231-1236.

Yokoyama, R., Shirasawa, M., Pike, R.J., 2002. Visualizing topography by openness: A new application of image processing to digital elevation models. Photogramm. Eng. Remote Sensing 68, 251-266.

Zakšek, K., Oštir, K., Kokalj, Ž., 2011. Sky-view factor as a relief visualization technique. Remote Sensing 3(2), 398-415.

Zevenbergen, L. W., Thorne, C. R., 1987. Quantitative analysis of land surface topography. Earth surface processes and landforms 12(1), 47-56.

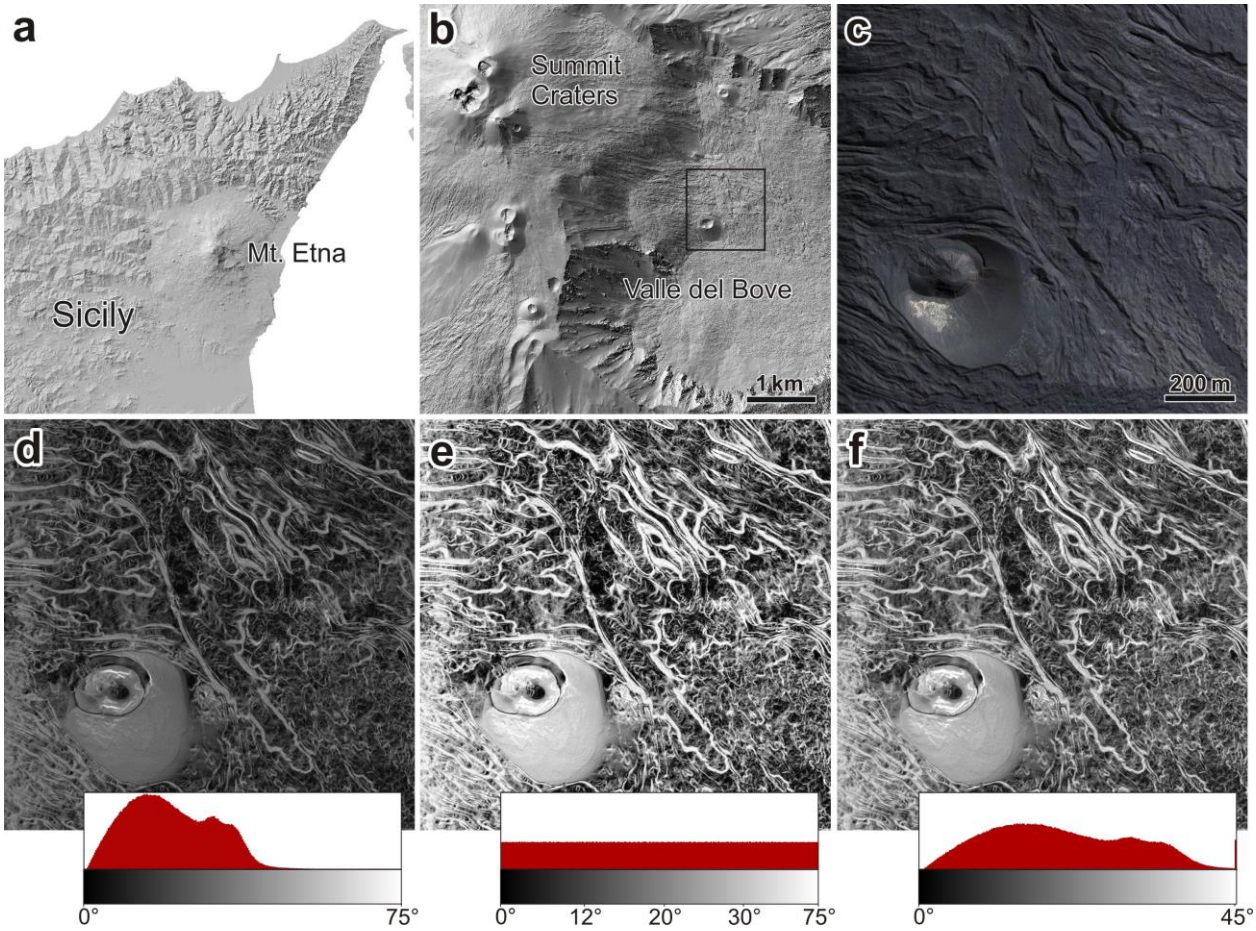

Fig. 1. Mount Etna test area. a) Hillshaded relief of northeast of Sicily Island with the location of Mt. Etna (Tarquini et al., 2012). b) Hillshaded relief of east flank of Mt. Etna; black contour shows the location of the test area. c) Aerial photo (downloaded from sif.regione.sicilia.it) of the test area with dimension of 1200 m × 1200 m. Frames d, e and f show grayscale image representations of the slope calculated from a high resolution DEM; insets display the histograms and legends of the slope maps (in degrees). d) Linear mapping of the (min, max) values of slope onto the (0, 255) intensity range of the gray tones: all slope values are faithfully represented but the image is poorly contrasted. e) Histogram equalization: the image has an optimal contrast but the form of the original histogram is completely lost and a correct display of the legend is very problematic. f) 2.5 σ histogram stretching: the image is well contrasted and the original shape of the most populated part of the histogram is maintained.

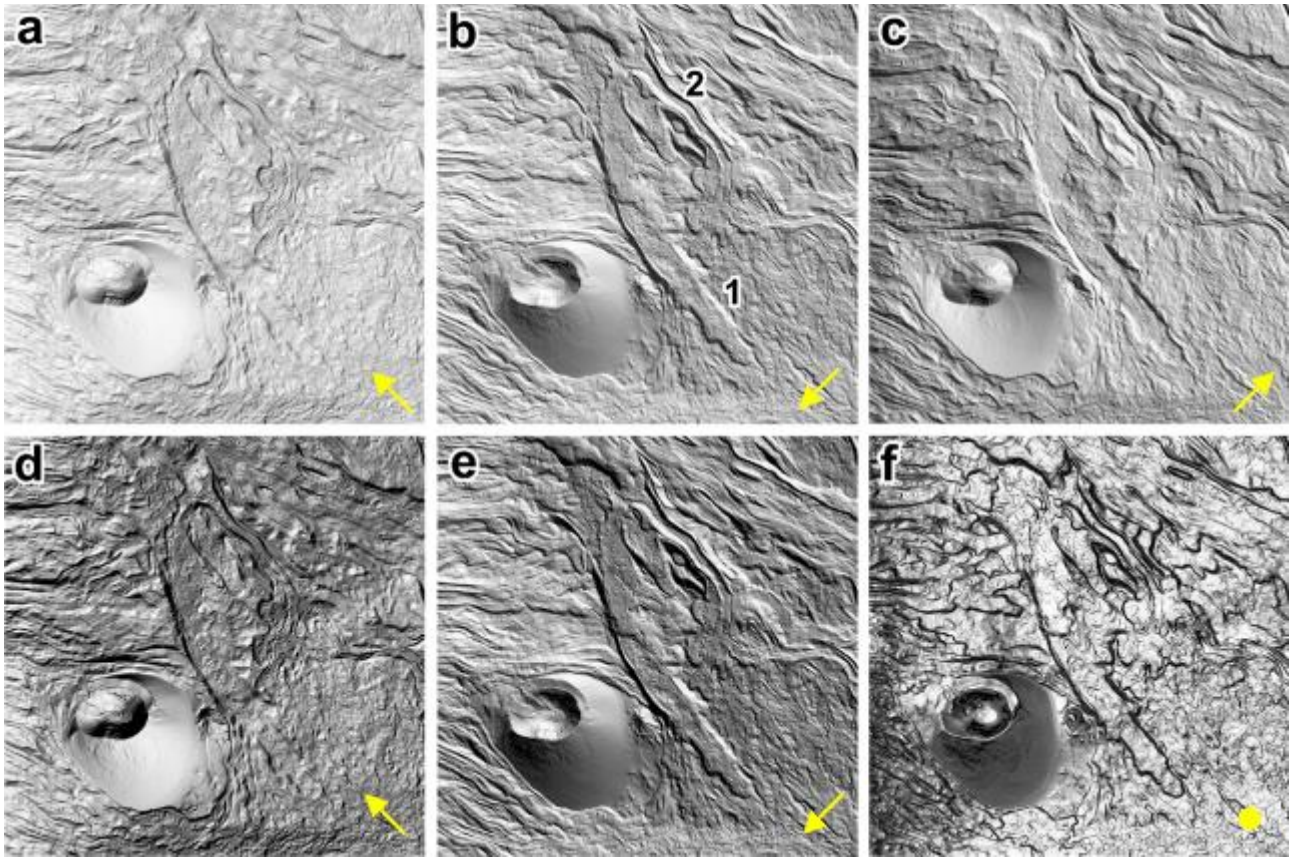

Fig. 2. Shaded relief maps of an area of 1200 m × 1200 m on Mt. Etna. Yellow arrows indicate the direction of illumination. a) Sun azimuth = 135°, sun elevation angle = 45°. b) Sun azimuth = 45°, sun elevation angle = 45°; label 1 identifies the terminal section of a lava flow and label 2 identifies a lava channel. c) Sun azimuth = 225°, sun elevation angle = 45°. d) Sun azimuth = 135°, sun elevation angle = 45°, 2.5 σ histogram stretching applied. e) Sun azimuth = 45°, sun elevation angle = 45°, 2.5 σ histogram stretching applied. f) Sun elevation angle = 90°, 2.5 σ histogram stretching applied. The angle of illumination, or azimuth, clearly affects the way features appear on shaded relief maps.

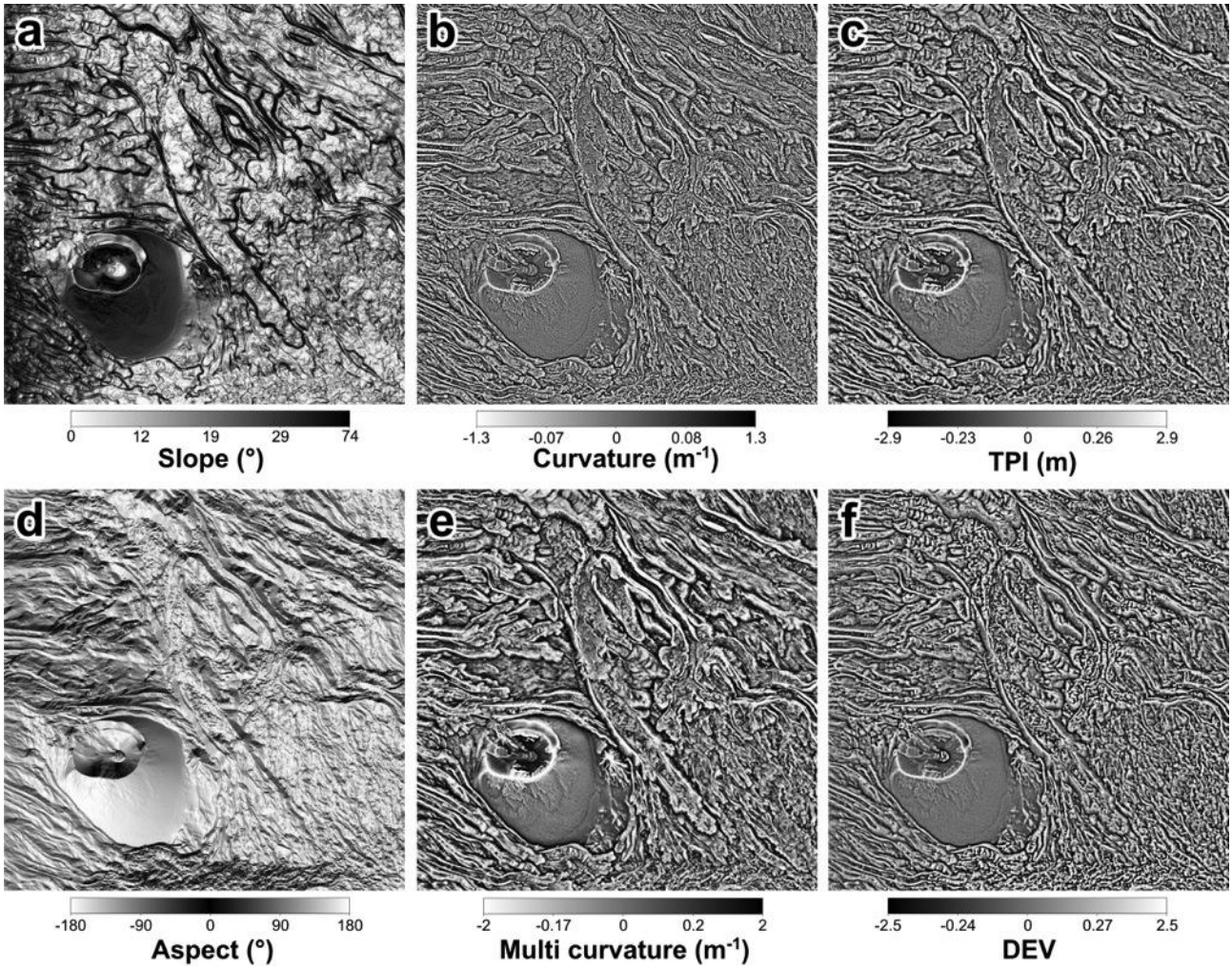

Fig. 3. Slope, aspect, curvature, *TPI* and DEV maps of an area of 1200 m × 1200 m on Mt. Etna. The simple curvature map is calculated at a length scale of 3 m, i.e. with a moving window of 3 × 3 pixels = 3 m × 3 m. The multi curvature example was obtained as the arithmetic average of the curvatures calculated at length scales of 3, 6, 12, 25, 50, and 100 m. *TPI* and *DEV* were calculated within a radius of 5 m.

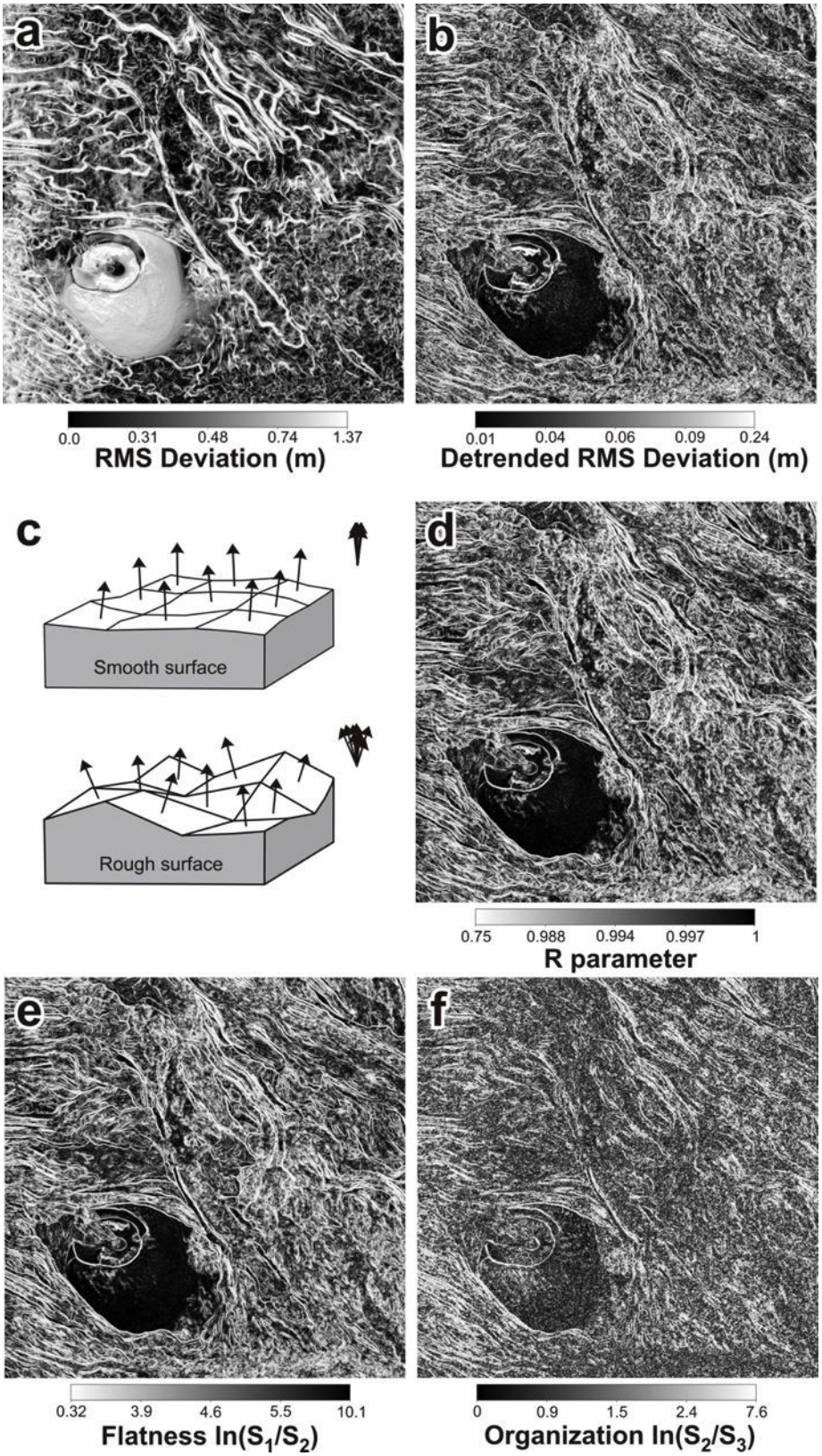

Fig. 4. Roughness maps for an area of 1200 m × 1200 m on Mt. Etna. a and b) The *RMS* Deviation (detrended and not) was calculated as explained in the main text with a radius of 2 m. c) Topographic surface roughness evidenced by unit normal vectors: smooth surfaces have coherent

orientations, whereas rough surfaces have a large degree of dispersion (modified from Coblentz and Karlstrom, 2011). d) *R* parameter, e) flatness $\ln(S_1/S_2)$ and f) organization $\ln(S_2/S_3)$ were calculated as explained in the main text with a sampling window of 5 × 5 cells = 5 m × 5 m.

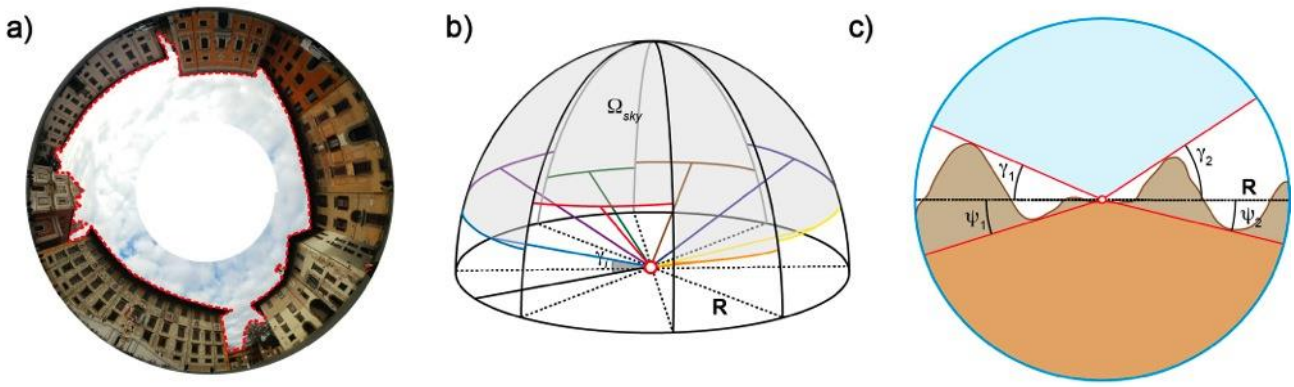

Fig. 5. The *SVF* is defined by the ratio of the solid angle (Ω_{sky}) of the visible sky above a certain observation point (dotted line in frame a). In frame a, the observation point is the middle of Piazza dei Cavalieri (Pisa, Italy) and the dotted line defines the border of the visible sky. In order to minimize the computing resources required, the *SVF* is calculated by computing the vertical elevation angle of the horizon γ_i in *n* directions (*n*=8 in frame b), limited to a specified radius R. In frame c, we show, for a given transversal section of the sphere, the definition of the γ_i and ψ_i angles used for the calculation of *SVF*, SFV2, mirrored *SVF*, openness, and openness up and down (after Zakšek et al., 2011).

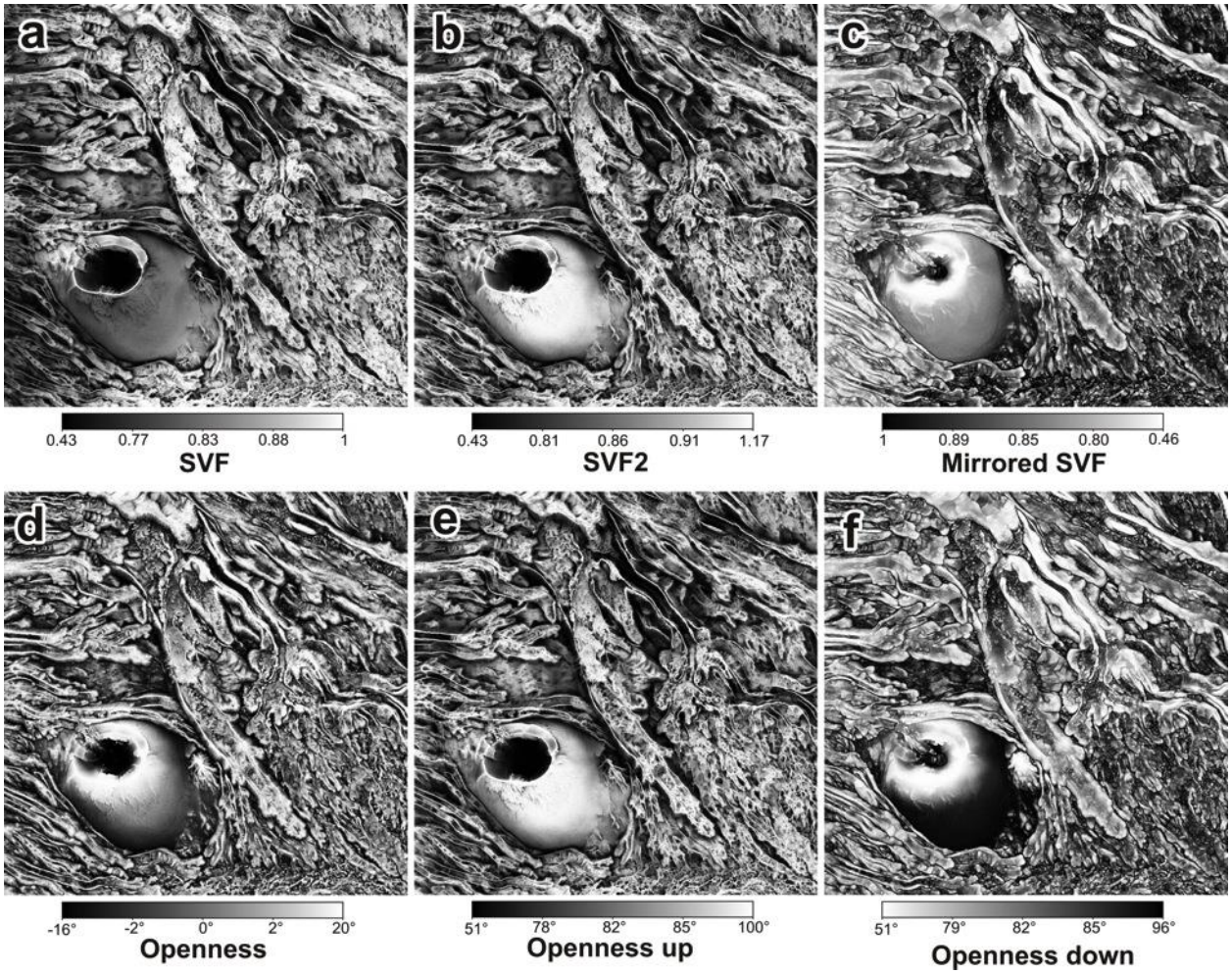

Fig. 6. Sky view factor (*SVF*) and openness maps for an area of 1200 m × 1200 m on Mt. Etna. *SVF*, *SVF*2 and mirrored *SVF* were computed using Eq. 12 (see main text for details). Mirrored *SVF* refers to the *SVF* of the DEM with opposite elevations values; openness up, openness down and openness were computed using Eqs. 13, 14 and 15, respectively. All calculations were performed along 8 search directions with a search radius of 100 m.

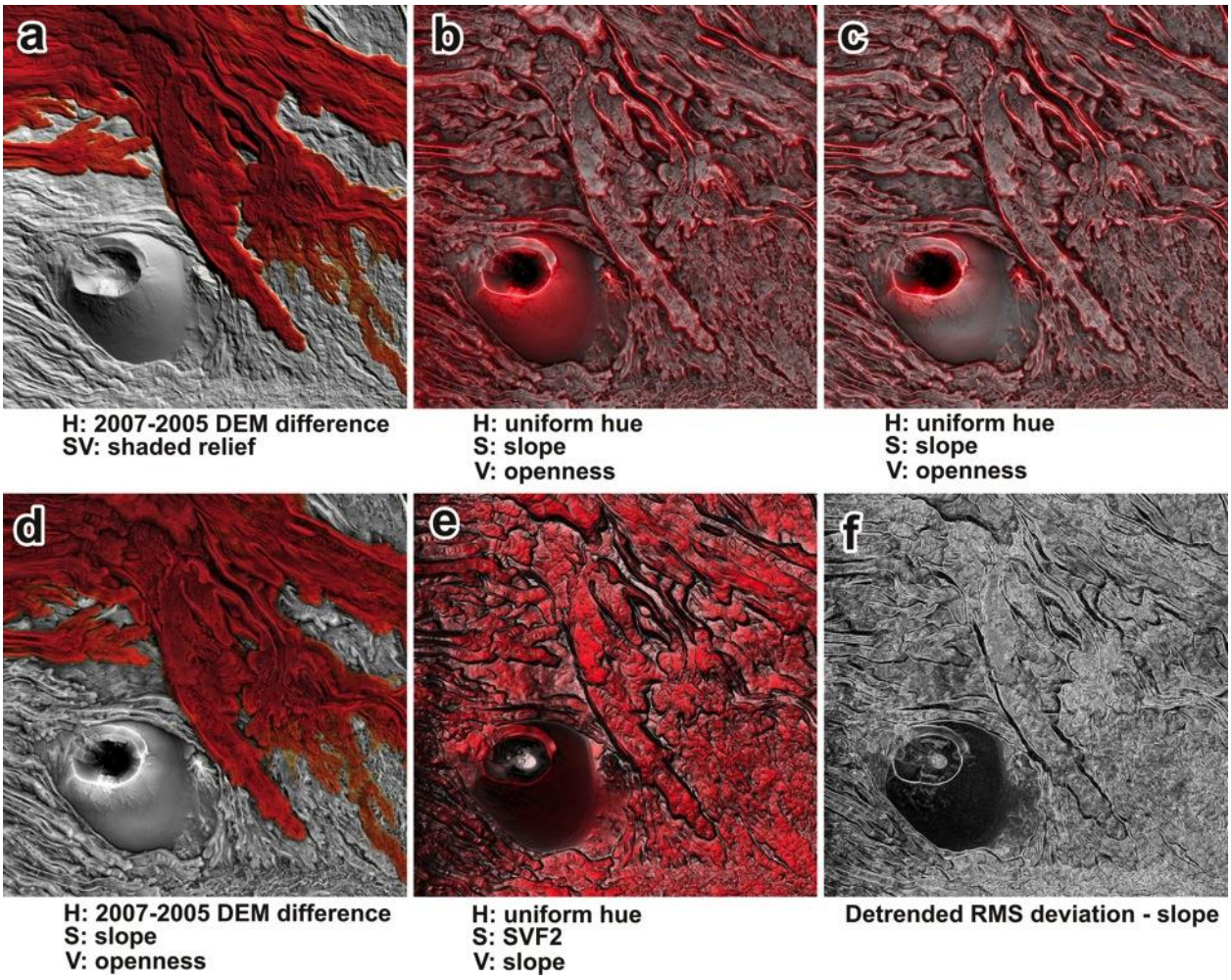

Fig. 7. Examples of map composition for an area of 1200 m × 1200 m on Mt. Etna. When applicable the map layers used for each channel of the HSV space is specified under the image. a) Standard colored thickness map overlaid onto a hill-shaded map. b) RRIM c) RRIM of *TPI* calculated within a radius of 120 m. d) RRIM with hues assigned according to the thickness of the lava flow emplaced in the period 2005-2007. e) HSV composition with *SVF*2 as saturation and slope as value. f) Image composition obtained applying a 2.5 σ histogram stretching to the difference between the detrended *RMS* deviation and the slope grids. For maps b) to e) the HSV composition is done using as input image layers with a 2.5 σ histogram stretching.

		DEM	Hill shading							«Curvatures»						Roughness						Openness						SVF			
			Hill-shaded 135° 45°	Hill-shaded 225° 45°	Hill-shaded 315° 45°	Hill-shaded 45° 45°	Hill-shaded indet. 90°	Slope	Aspect	Curvature	Multi curvature	TPI - 2 pix	TPI - 100 pix	DEV - 2 pix	DEV - 100 pix	RMS Deviation - 2 pix	RMS Deviation - 3 pix	$\ln(S_1/S_2)$ - 5 pix	$\ln(S_1/S_3)$ - 5 pix	$\ln(S_2/S_3)$ - 5 pix	Parameter R - 5 pix	Openness down - 20 pix	Openness down - 100 pix	Openness up - 20 pix	Openness up - 100 pix	Openness - 20 pix	Openness - 100 pix	SVF - 20 pix	SVF - 100 pix	SVF2 - 20 pix	SVF2 - 100 pix
SVF	SVF2 - 100 pix	1	6	1			15	13		29	41	29	27	22	26	6	8	5	2		3	8	2	79	99	49	58	67	80	79	
	SVF2 - 20 pix		2				5	5		47	64	46	15	36	17	5	7	7	4		4	19	9	99	78	72	63	66	60		79
	SVF - 100 pix	8		4	11	1	40	40		24	33	23	15	18	16	5	6	2		2	2	7		61	81	38	42	90		60	80
	SVF - 20 pix	6		4	16	1	42	43		30	39	29	7	24	8	5	7	2		2	3	9		67	68	43	38		90	66	67
Openness	Openness - 100 pix									52	73	51	49	39	48							60	56	62	57	86		38	42	63	58
	Openness - 20 pix									67	90	66	21	50	23							71	48	72	49		86	43	38	72	49
	Openness up - 100 pix	1	6	1			16	14		29	41	28	26	22	26	6	8	5	2		4	8	2	79		49	57	68	81	78	99
	Openness up - 20 pix		2				6	5		47	64	46	15	35	16	6	7	7	4	1	4	18	9		79	72	62	67	61	99	79
	Openness down - 100 pix	4	6	1			16	14		30	42	30	29	22	28	4	6	3	2		3	78		9	2	48	56			9	2
	Openness down - 20 pix		3				5	5		48	65	47	14	35	16	4	6	5	3		3		78	18	8	71	60	9	7	19	8
Roughness	Parameter R - 5 pix															80	85	65	20	25		3	3	4	4			3	2	4	3
	$\ln(S_2/S_3)$ - 5 pix															24	28	35	10		25			1				2	2		
	$\ln(S_1/S_3)$ - 5 pix		2		3		1	1								26	27	34		10	20	3	2	4	2					4	2
	$\ln(S_1/S_2)$ - 5 pix				1											73	80		34	35	65	5	3	7	5			2	2	7	5
	RMS Deviation - 3 pix							1								89		80	27	28	85	6	6	7	8			7	6	7	8
	RMS Deviation - 2 pix																89	73	26	24	80	4	4	6	6			5	5	5	6
«Curvatures»	DEV - 100 pix	1								5	14	5	87	4								16	28	16	26	23	48	8	16	17	26
	DEV - 2 pix									73	63	73	3		4							35	22	35	22	50	39	24	18	36	22
	TPI - 100 pix									5	12	5		3	87							14	29	15	26	21	49	7	15	15	27
	TPI - 2 pix									99	88		5	73	5							47	30	46	28	66	51	29	23	46	29
	Multi curvature									89		88	12	63	14							65	42	64	41	90	73	39	33	64	41
	curvature										89	99	5	73	5							48	30	47	29	67	52	30	24	47	29
	aspect	3		49		47																									
	slope	8	1	8	42	4	94										1		1			5	14	5	14			43	40	5	13
Hill shading	Hill-shaded indet. 90°	8		8	39	5		94											1			5	16	6	16			42	40	5	15
	Hill-shaded 45° 45°	1	2	77	5		5	4	47																			1	1		
	Hill-shaded 315° 45°	5	67			5	39	42										1	3									16	11		
	Hill-shaded 225° 45°	6	1			77	8	8	49														1		1			4	4		1
	Hill-shaded 135° 45°			1	67	2		1											2			3	6	2	6					2	6
	DEM			6	5	1	8	8	3						1								4		1			6	8		1

0 - 0.01 | 0.01 - 0.1 | 0.1- 0.2 | 0.2 - 0.4 | 0.4 - 0.6 | 0.6 - 0.9 | 0.9 - 1 | 1

Fig. 8. Matrix of the squared correlations between the quantities illustrated in Fig. 2, 3, 4, and 6. The numbers inside the cells is the square correlation expressed as percentage. Length scale, when necessary, follows the quantity name and is reported in pixel units (pix; in this case 1 pix = 1 m). For the openness and *SVF* quantities the searching radius is reported. For the *RMS* deviations the radius of the neighborhood is reported and for the other roughness parameters the moving window linear dimension is reported: e.g. "parameter R – 5 pix" means that the parameter R has been calculated with a moving window 5×5 pixels.

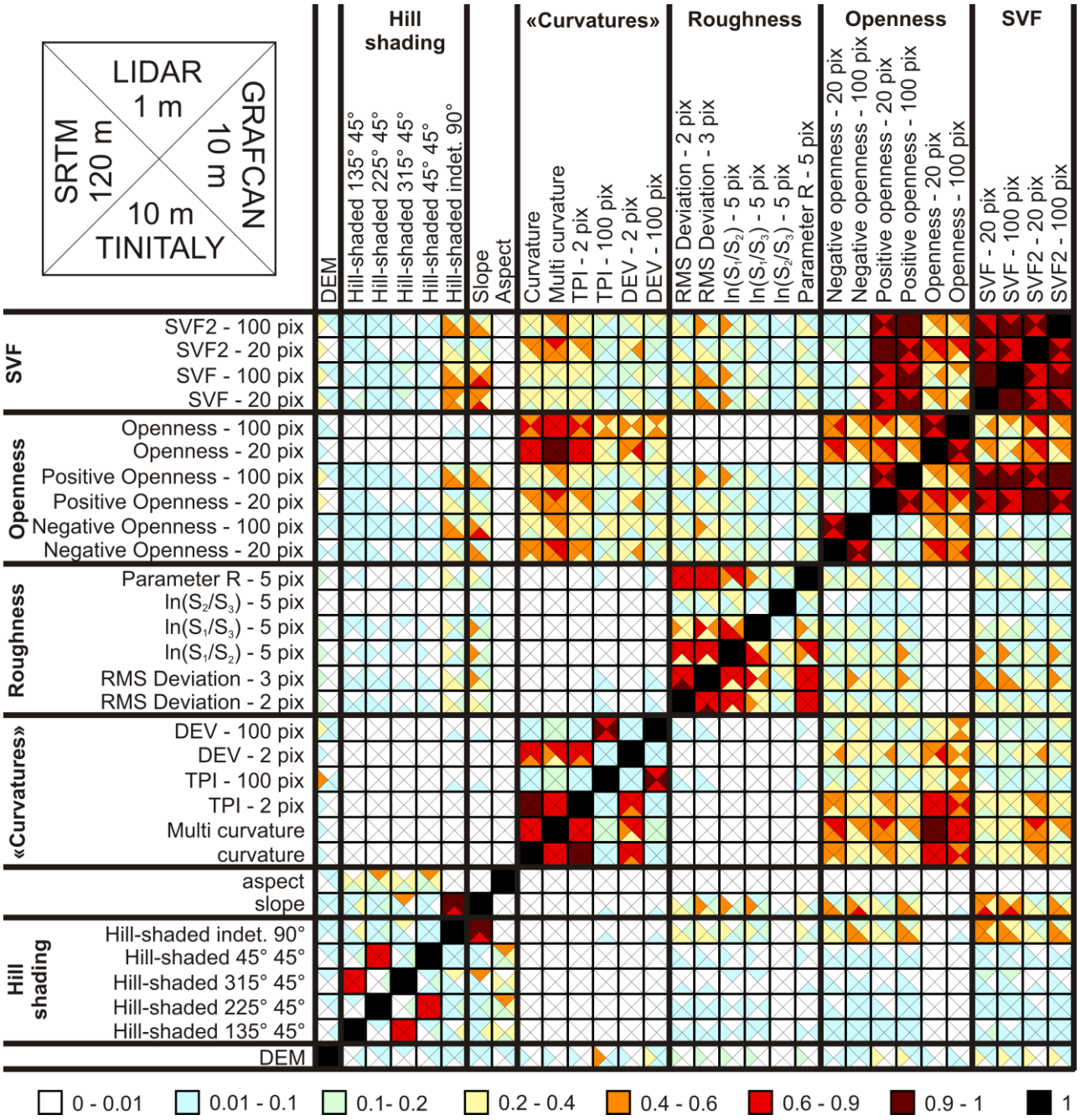

Fig. 9. Matrix of the squared correlations among the quantities considered in this paper. Each matrix element is split in four triangular sub-elements corresponding to different areas and DEMs. The upper sub-element refers to 1-m resolution LiDAR DEM of a portion of Mt. Etna. The lower sub-element refers to a 10–m resolution 2005 DEM of Etna region (Italy) produced by the merge of a 1-m LIDAR DEM (Favalli et al. 2009) and TINITALY DEM (Tarquini et al., 2012). The right sub-element refers to the 10-m resolution DEM of Tenerife Island (Canary Islands, Spain) produced

by GRAFCAN (2009). The left sub-element refers to the SRTM DEM, resampled to 120 m, of a region of Ethiopia. Length scale, when necessary, follows the quantity name and is reported in pixel units. For the openness and *SVF* quantities the searching radius is reported. For the *RMS* deviations the radius of the neighborhood is reported and for the other roughness parameters the moving window linear dimension is reported: e.g. “parameter R – 5 pix” means that the parameter R has been calculated with a moving window 5×5 pixels.

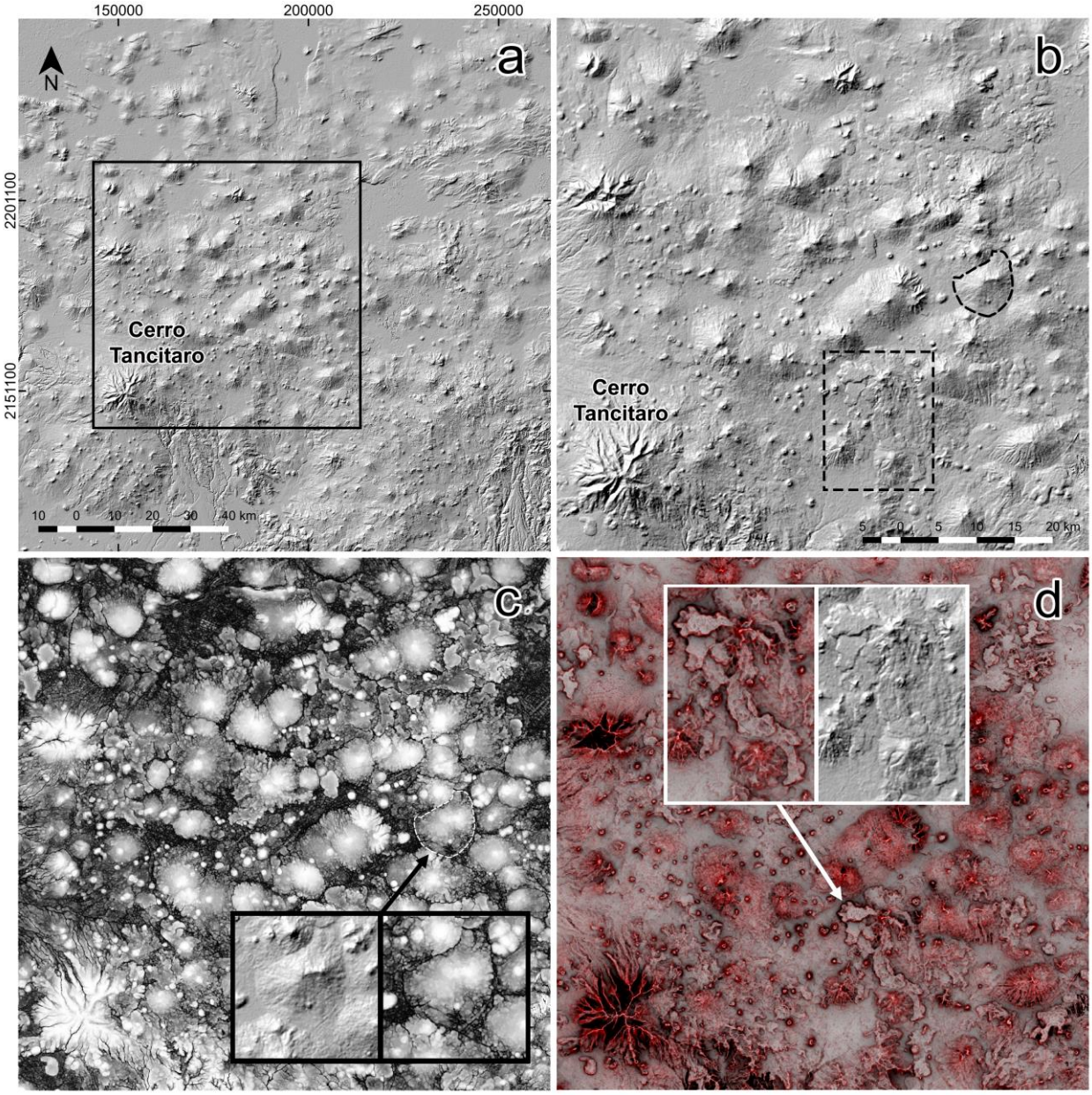

Fig. 10. DEM-derived maps used for interpreting the Michoacán-Guanajuato volcanic field morphologies. a) Overview of the investigated area represented by the hill-shaded map. The square box outlines the area shown in the frames b, c and d; b) Hill-shaded map giving immediate insight into the morphological complexity of this area, but not allowing to easily distinguish between neighboring volcanic features. A volcanic edifice and a lava flow are selected as examples. c) Openness down map which helps to identify the base of adjacent cones, as shown in the inset where the hillshading and openness down maps are compared for the selected cone. d) "RRIM style" map built with slope and *SVF*, which are largely uncorrelated, allows one to recognize effectively the complex superimposition of volcanic products as highlighted in the inset for the selected lava flow.

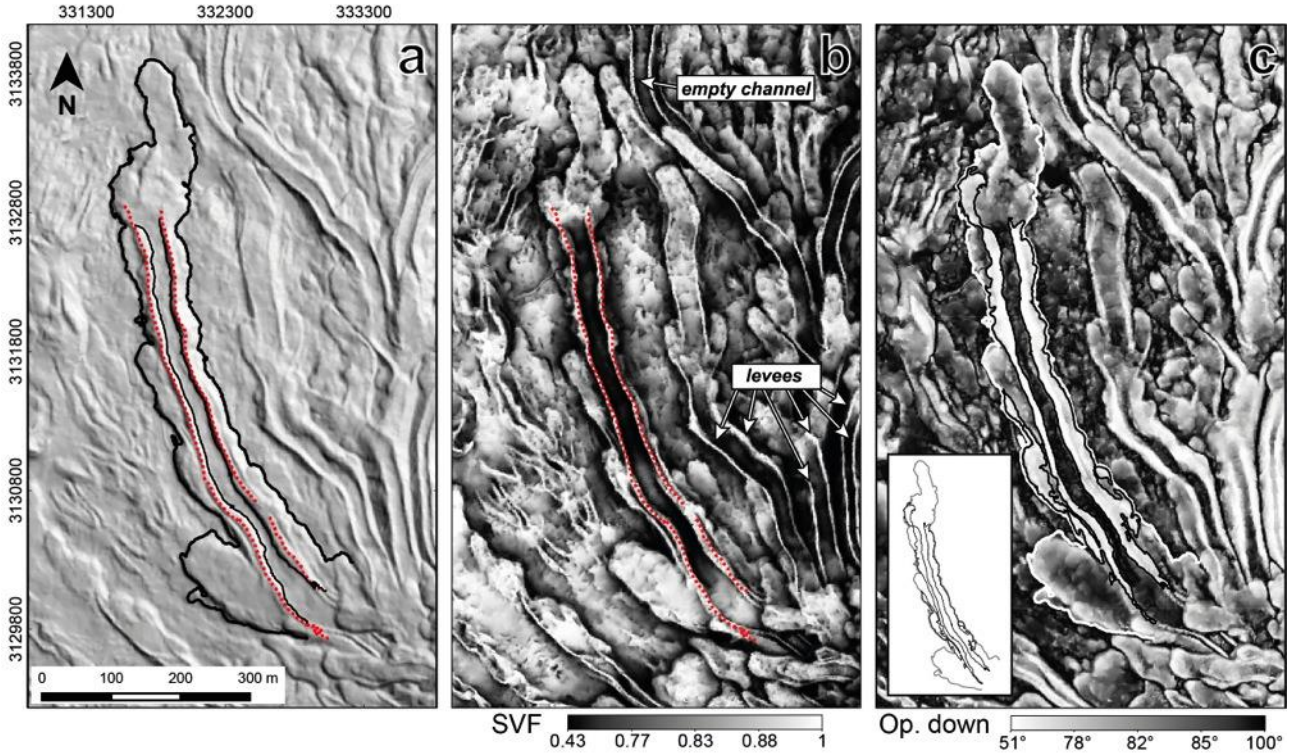

Fig. 11. Extraction of the main features from a lava channel belonging to the Roques Blancos lava flow (Tenerife Island). a) Hillshaded map with lines defining the base of the lava (external continuous line), the levees (dotted lines) and the base of the channel (internal continuous lines) extracted in a semi-automatic way from the openness down and hillshaded maps. b) *SVF* map which allows identification, with great accuracy, of the channel levees and the features inside them. c) Openness down map which can be used to distinguish among different lava flows because it highlights the particular slope breaks occurring between a lava flow and the substrate. For the same reason it highlights the contacts between internal levees and the base of the channel. Also in this case, with appropriate values used, the base of the lava (white line in the figure and gray in the inset) and the internal channel (black lines in the figure and inset) can be semi-automatically extracted.